Robust Bone Detection in Ultrasound Using Combined Strain Imaging and Envelope Signal Power Detection

Mohammad Arafat Hussain[1], Antony Hodgson[2], and Rafeef Abugharbieh[1]

[1] Department of Electrical and Computer Engineering
[2] Department of Mechanical Engineering, The University of British Columbia, Vancouver, BC, Canada
{arafat,rafeef}@ece.ubc.ca, ahodgson@mech.ubc.ca

Abstract. Bone localization in ultrasound (US) remains challenging despite encouraging advances. Current methods, e.g. local image phase-based feature analysis, showed promising results but remain reliant on delicate parameter selection processes and prone to errors at confounding soft tissue interfaces of similar appearance to bone interfaces. We propose a different approach combining US strain imaging and envelope power detection at each radio-frequency (RF) sample. After initial estimation of strain and envelope power maps, we modify their dynamic ranges into a modified strain map (MSM) and a modified envelope map (MEM) that we subsequently fuse into a single combined map that we show corresponds robustly to actual bone boundaries. Our quantitative results demonstrate a marked reduction in false positive responses at soft tissue interfaces and an increase in bone delineation accuracy. Comparisons to the state-of-the-art on a finite-element-modelling (FEM) phantom and fiducial-based experimental phantom show an average improvement in mean absolute error (MAE) between actual and estimated bone boundaries of 32% and 14%, respectively. We also demonstrate an average reduction in false bone responses of 87% and 56%, respectively. Finally, we qualitatively validate on clinical in vivo data of the human radius and ulna bones, and demonstrate similar improvements to those observed on phantoms.

Keywords: Ultrasound, bone, strain imaging, segmentation.

1 Introduction

Fluoroscopy remains the primary intraoperative imaging modality for bone boundary visualization in computer assisted orthopaedic surgery systems. The associated radiation exposure posing risks to both patients and surgical teams gave rise to recent interest in safer non-ionizing real-time intraoperative imaging alternatives such as US [1].

In US guided surgical intervention, bone localization in US images is essential for visualization and guidance, e.g. during fragment positioning in fracture reduction surgeries [1]. Despite recent advancement in US intensity-based automatic

P. Golland et al. (Eds.): MICCAI 2014, Part I, LNCS 8673, pp. 356–363, 2014.

bone segmentation, results remain unpredictable due to the high levels of speckle noise, reverberation, and signal drop out [1]. Recent work by Hacihaliloglu et. al. [2] on local image phase feature-based bone segmentation addressed some of these limitations however remains prone to false positive bone responses at soft tissue interfaces that commonly exhibit similar intensity profiles as bone interfaces.

Elastography is an emerging medical diagnostic tool for capturing the mechanical properties (e.g. stiffness) of biological tissue [3]. Elastography has shown promise in the detection of breast and prostate tumors, liver cirrhosis, vascular plaques [3], and ligament-bone insertion. However, in the bone imaging literature, US elastography has been very limited. In [4], bone detection using US elastography was investigated. The reported strain images, however, showed low contrast between the hard bone and soft tissue regions. In addition, problems arose from signal windowing as window-based elastography (WBE) methods have limitations associated with the size of the window segments. A significant amount of noise in the strain image can be easily introduced with the choice of smaller window size and/or large overlap between successive windows [3].

In this paper, we propose a novel method for robust bone boundary localization based on combined US strain imaging and envelope power signal detection. Our method uses real-time strain imaging based on analytic minimization (AM) of regularized cost functions [5]. The AM method estimates strain for each of the RF samples, so the resulting strain image has better spatial resolution than that of the WBE methods, and does not suffer from window-related artifacts. Furthermore, WBE methods often produce distorted strain estimates due to the amplitude modulation effect even if there is no displacement estimation error [6]. In contrast, the cost functions used in the AM method incorporate a measure of the similarity of RF data intensity as well as displacement continuity, which makes the method robust to echo de-correlations present throughout the image; in turn, this produces smoother transitions across bone/soft tissue interfaces. To better delineate the bone boundary, we combine the envelope power map with the strain image. We use the envelope power map rather than an envelope or log-compressed envelope map (i.e. B-mode) as it possesses a higher dynamic range. As elastography estimates tissue stiffness, we achieve a marked reduction of false positive bone responses at the soft tissue interfaces.

2 Methods

Our method is divided into three parts. In Sect. 2.1, we discuss the strain map estimation and subsequent processing of it. Then, in Sect. 2.2, we discuss the estimation of the envelope power map and its further processing. Finally, in Sect. 2.3, we discuss our integration procedure of the strain and envelope power maps.

2.1 Estimation of Modified Strain Map (MSM)

The AM-based strain estimation method has been described in detail elsewhere [5]. However, in brief, the AM method estimates tissue displacement from the

pre- and post-compression RF echo frames using a regularized cost function that incorporates three regularizing parameters and representations of the estimated axial and lateral displacements. The cost function is partial-differentiated with respect to the displacements and set to zero. Assumptions related to the depth dependence of US attenuation, the size of lateral displacements and the displacement at the transducer face are introduced to simplify the solution of the problem, and a Kalman filter-based method is adopted to estimate the final strain $\mathbf{S}$ from the estimated displacement map [5]. Finally, to produce a strain map with a dynamic range roughly equivalent to that of the envelope power map, we estimate the MSM $= \hat{\mathbf{S}}/\hat{\mathbf{S}}_M$, where $\hat{\mathbf{S}} =\mid (-\mathbf{S})+ \mid median(-\mathbf{S}) \mid\mid$, $\hat{\mathbf{S}}_M$ is the maximum of $\hat{\mathbf{S}}$, and *median* is the median operator.

2.2 Estimation of Modified Envelope Map (MEM)

As the strain is mapped with respect to the pre-compression RF frame, we use the same pre-compression RF frame to generate the MEM so that it can be spatially matched to the MSM. The envelope of a RF scan-line at column j is calculated as $\mathbf{E}_j(i) =\mid H[I_{1,j}(i)] \mid$ [7], where H denotes the Hilbert transform. Finally, we estimate MEM $= \hat{\mathbf{E}}/\hat{\mathbf{E}}_M$, where $\hat{\mathbf{E}} = \mathbf{E}^2$ and $\hat{\mathbf{E}}_M$ is the maximum of $\hat{\mathbf{E}}$.

2.3 Fused Map (FM) Estimation and Bone Boundary Localization

Our final step involves fusing the MSM and MEM into a single FM measure as

$$\text{FM} = \lambda \times \text{MSM} + (1 - \lambda) \times \text{MEM}, \tag{1}$$

where λ is the weight. To choose a suitable value of λ, we analyse the effect of this choice on the accuracy of the bone boundary localization in an FEM-based simulation of a noisy environment (i.e. 10dB SNR). Fig. 1(h) shows the MAE as a function of different values of λ ranging from 0.3 to 0.7. From this figure we see that the mean MAE is minimized for $\lambda = 0.5$. While this value for λ may not be optimal under all possible imaging situations, the results seem to be relatively insensitive to this choice, so we opted to set $\lambda = 0.5$ for this study. However, after estimating the FM, the maximum intensity point along each scan-line of the FM is detected and the final bone boundary is estimated using a local linear-fit with a length of 3mm over the detected intensity points.

3 Validation Setup

Simulated Phantom. We built a 40mm×40mm FEM phantom using the ANSYS analysis software (ANSYS, Inc., Canonsburg, PA) and then generated an ultrasound simulation of the model using Field II [8]. Our phantom mimicked an US scan of the human distal radius bone with a total number of nodes of 55,180. The stiffness of the homogeneous soft tissue and bone region were set to

10kPa and 10GPa, respectively as previously reported in the literature [9]. Our phantom was compressed from the top using a larger-width planar compressor in free-hand fashion. An ultrasonic transducer of center frequency, $f_0 = 5$MHz and band-width = 50% was used to simulate the phantom scan from the top. The total number of scan lines was set to 128. We set an applied pressure level that corresponds to 1% average strain. In addition, we did not model out-of-plane motion.

Experimental Physical Phantom. We constructed an experimental phantom using a radio-opaque Sawbones hemi-pelvis (Sawbones, Pacific Research Laboratories, Inc., Vashon Island, WA), model number 1297-22. A portion of the pelvis was suspended in a PVC gel and placed in an acrylic tube. A high resolution peripheral quantitative computed tomography (CT) machine, model HR pQCT Xtreme CT (Scanco USA, Inc., Wayne, PA) was used to acquire a single 482×482×402 (lateral×axial×elevational) voxel volume with a resolution of 0.25mm^2. In addition, US was acquired using a SonixRP (Ultrasonix Medical Corporation, Richmond, BC) scanner integrated with a L14-5W/60 probe operating at 10MHz.

Real In Vivo Data. We acquired three sets of in vivo US data with free-hand compression from three volunteers (volunteer-I: 25-year old male; volunteer-II: 26-year old male; volunteer-III: 24-year old male) after proper prior consent was obtained. US was acquired using a SonixRP (Ultrasonix Medical Corporation, Richmond, BC) scanner integrated with a L14-5W/60 probe operating at 10MHz. The study was approved by our institutional review board (IRB).

4 Results and Discussion

We provide comparative results of our proposed method with the automatic adaptive parameterization in local phase feature-based bone segmentation in US (APS) [2] method using the FEM phantom, experimental phantom and in vivo data. The initial parameters in the APS method are chosen according to [2] such that the best possible bone map is generated. We calculate MAE that is defined as MAE $= \frac{1}{N}\sum_{k=1}^{N} \mid A(k) - G(k) \mid$, where N is the approximated number of columns on which the bone boundary spans, A is the matrix containing the actual bone boundary points (ground truth), and G is the matrix containing the estimated bone boundary points. As ground truth, we use the estimated bone boundaries from the ideal elastogram and CT image for the FEM and experimental phantom, respectively. We also estimate mean signed distance (MSD) [2] for quantitative evaluation of the false positive responses produced by the proposed and APS method using the FEM and experimental phantom data. Signed distance of a bone response in any scan-line is estimated with respect to the actual bone position along that particular scan-line. Note that to estimate MSD for the proposed method, we use the bone boundary points before applying the regression.

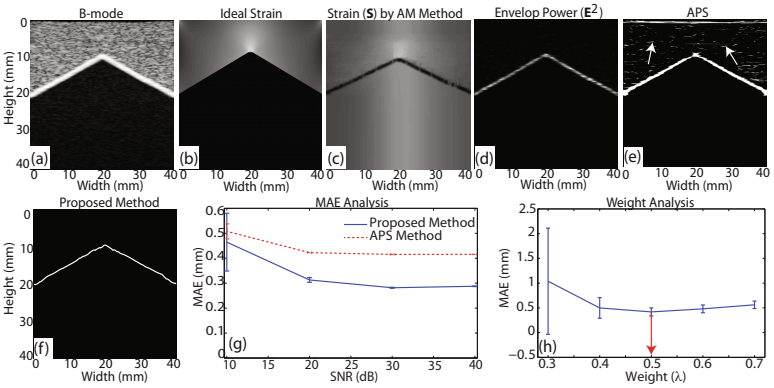

Fig. 1. Illustration of bone boundary detection using the FEM phantom. (a) B-mode image, (b) ideal strain image, (c) strain image $\mathbf{S}$ generated by the AM method, (d) envelop power map $\hat{\mathbf{E}}$, (e) estimated bone boundary by the APS method, (f) estimated bone boundary by the proposed method, (g) MAE analysis of the proposed and APS methods at different SNRs, and (h) weight analysis at 10dB SNR (weight at minimum error is shown with red arrow).

FEM Results. We provide comparative qualitative and quantitative results of our proposed and APS method using the FEM data. In Figs. 1(a), (b), (c) and (d), we show the B-mode, ideal strain, estimated strain $\mathbf{S}$, and envelop power $\hat{\mathbf{E}}$ images, respectively. Note that we are dealing with anatomy that includes bone, hence, the RF intensities fall sharply (compared to soft tissue) beneath the bone surface. In such a situation, the regularization terms in the cost equation become larger than the signal part in the region beneath the bone surface and over-smoothing tends to occur [5]. In Figs. 1(e) and (f), we show the bone boundaries detected by the APS and proposed methods, respectively. The figures demonstrate that the APS method produces several false positive bone responses (indicated by white arrows) due to the presence of ridge-like features in the B-mode image. In contrast, the bone boundary produced by our method (Fig. 1(f)) is apparently free of such artifacts. Note that if the false positive responses produced by the APS method could be ignored, then a local fitting over the actual bone responses similar to the proposed method could produce better bone boundary. We also compare the quantitative performance of the proposed and APS methods in terms of MAE in Fig. 1(g) with four different signal-to-noise ratio (SNR) simulations (40, 30, 20, and 10dB) with 100 realizations each. As can be seen in this figure, up to 20dB SNR, the APS method produces greater mean MAE than that of the proposed method, though the mean MAE of both the methods are almost flat and standard deviations (SD) are close to zero. In addition, the mean MAE of the APS method at 10dB SNR is higher though the SD of the proposed method in this case somewhat higher. Moreover, the estimated MSDs are found to be 0.68 ± 2.5mm and 5.47 ± 6.20mm for the proposed and APS methods, respectively. Therefore, we can say that the proposed method shows better performance in terms of reduced false positive bone responses than that of the APS method.

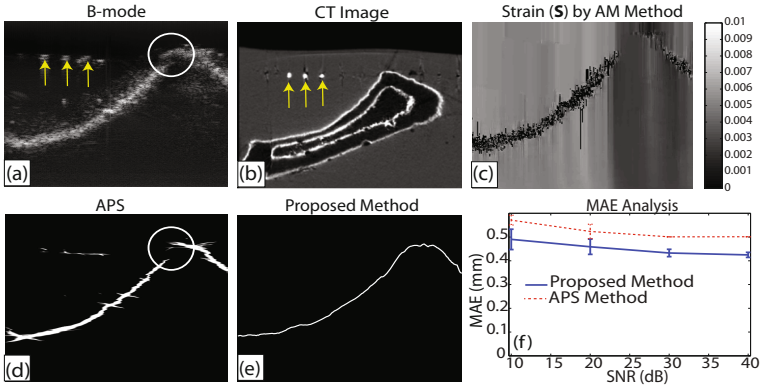

Fig. 2. Illustration of the bone boundary detection using the experimental phantom. (a) B-mode image, (b) a CT projection along which US scanning is performed, (c) strain image **S**, (d) estimated bone boundary by the APS method, (e) estimated bone boundary by the proposed method, and (f) MAE analysis of the proposed and APS methods at different SNRs.

Experimental Phantom Results. Figure 2 demonstrates the qualitative and quantitative performance comparison of the proposed and APS methods using the experimental phantom. In Fig. 2(a), we show the B-mode image. Figure 2(b) shows the CT projection slice along which the US scanning is performed and fiducials in Fig. 2(a) corresponds to fiducials in Fig. 2(b) (shown with yellow arrows) in the same order. The estimated strain image is shown in Fig. 2(c). We show the detected bone boundaries by the APS and proposed methods in Figs. 2(d) and (e), respectively. We can see from Fig. 2(d) that the bone boundary image estimated by the APS method produces false positive responses in soft tissue regions and fails to estimate bone boundary where US back-scatter response is very weak (shown with white circles in Figs. 2(a) and (d)). In contrast, the bone boundary estimated by the proposed method has no discontinuity as well as produces no noticeable false positive response. We also show the quantitative performance of both the methods in Fig. 2(f). Here too, we use four different SNRs (40, 30, 20, and 10dB) with 100 realizations for each of them to analyze the MAE. Since the quality of the ultrasound machine-acquired RF data is dependent on user-defined parameters, the signals may have different signal to noise ratios in different situations. Therefore, we have used a range of SNRs to evaluate the robustness of our proposed scheme. We can see from this figure that the mean MAE values of the proposed method are lower than that of the APS method at all SNRs though the SDs of the proposed method are slightly higher. In addition, the estimated MSDs are found to be 0.66 ± 0.64mm and 1.51 ± 3.34mm for the proposed and APS methods, respectively. Therefore, from here too, we can say that the proposed method shows better performance in terms of reduced false positive bone responses than that of the APS method.

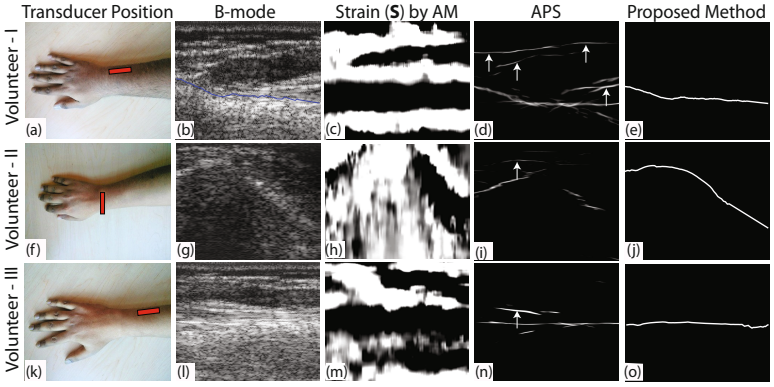

Fig. 3. Illustration of the bone boundary detection using the in vivo data. (a), (f) and (k) show the transducer face positions on each volunteer's hand (with red rectangles), (b), (g) and (l) are the B-mode images, (c), (h) and (m) are strain images **S**, (d), (i) and (n) show the detected bone boundaries by the APS method, and (e), (j) and (o) are the detected bone boundaries by the proposed method.

In Vivo Results. We compared the bone boundary detection performance of our proposed and APS methods using the in vivo data. The transducer positions on the anatomies as well as the B-mode images of volunteer-I, II and III are shown in Figs. 3(a) and (b), (f) and (g), and (k) and (l), respectively. Note that for volunteer-II, only half of the total scan-lines are considered for both methods since almost half of the transducer face laterally was in the air. We can see from Figs. 3(d), (i) and (n) that the APS method produced false positive response for bone in the soft tissue interfaces (shown with white arrows). In addition, in Fig. 3(i), the APS method fails to show the bone boundary. In contrast, in all three cases, the bone boundaries estimated by our proposed method better match the shapes visible in the corresponding B-mode images. (see Figs. 3(e), (j) and (o)). In addition, our method did not produce false positives at soft tissue interfaces.

5 Conclusions

We proposed a novel method for robust bone boundary localization based on the fusion of strain imaging and envelope signal power detection. We combined real-time strain imaging based on analytic minimization of regularized cost functions with an envelope power map of the pre-compression RF frame. Our results demonstrated reduced bone localization error through better elastogram resolution, adoption of envelope power map of higher dynamic range, addressing the false positive bone response, and exploiting the smoothing feature of the AM method to better delineate the bone boundary in strain image. We demonstrated our improved performance on a wide range of validation data including a simulated FEM phantom, a physical experimental phantom, and in vivo data of the human with reported improvements of approximately 32% and 14% in

terms of MAE, and 87% and 56% in terms of MSD in the FEM and experimental phantom tests, respectively, when compared with current state-of-the-art. We plan to follow up this promising initial study with a more extensive range of clinical test cases to better identify situations in which our method does not produce accurate results. We anticipate that it will be more problematic in situations where the bone boundary lies relatively far below the skin surface due to signal dropout and inhomogeneous tissue deformation near the bone boundary. However, preliminary indications are that the technique is quite robust when the bone boundary lies close to the skin surface.

References

1. Hacihaliloglu, I., Abugharbieh, R., Hodgson, A.J., Rohling, R.N.: Bone Segmentation and Fracture Detection in Ultrasound Using 3D Local Phase Features. In: Metaxas, D., Axel, L., Fichtinger, G., Székely, G. (eds.) MICCAI 2008, Part I. LNCS, vol. 5241, pp. 287–295. Springer, Heidelberg (2008)
2. Hacihaliloglu, I., Abugharbieh, R., Hodgson, A.J., Rohling, R.N.: Automatic Adaptive Parameterization in Local Phase Feature-based Bone Segmentation in Ultrasound. Ultrasound in Med. and Biol. 37(10), 1689–1703 (2011)
3. Hussain, M.A., Anas, E.M.A., Alam, S.K., Lee, S.Y., Hasan, M.K.: Direct and Gradient Based Average Strain Estimation by Using Weighted Nearest Neighbor Cross-correlation Peaks. IEEE Trans. Ultra. Ferro. Freq. Cont. 59(8), 1713–1728 (2012)
4. Wen, X., Salcudean, S.E.: Enhancement of Bone Surface Visualization Using Ultrasound Radio-frequency Signals. In: IEEE Ultra. Symp., vol. 1051, pp. 2535–2538 (2007)
5. Rivaz, H., Boctor, E.M., Choti, M.A., Hager, G.D.: Real-time Regularized Ultrasound Elastography. IEEE Trans. Med. Imag. 30(4), 928–945 (2011)
6. Lindop, J.E., Treece, G.M., Gee, A.H., Prager, R.W.: Estimation of Displacement Location for Enhanced Strain Imaging. IEEE Trans. Ultra. Ferro. Freq. Cont. 54(9), 1751–1771 (2007)
7. Hussain, M.A., Alam, S.K., Lee, S.Y., Hasan, M.K.: A Robust Strain Estimation Algorithm Using Combined Radio-frequency and Envelope Cross-correlation with Diffusion Filtering. Ultrason. Imag. 34(2), 93–109 (2012)
8. Jensen, J.A.: Field: A Program for Simulating Ultrasound Systems. In: 10th Nordicbaltic Conf. on Biomed. Imag. Part I, vol. 4(1), pp. 351–353 (1996)
9. Pistoia, W., Rietbergen, B.V., Lochmüller, E., Lill, C.A., Eckstein, F., Rüegsegger, P.: Estimation of Distal Radius Failure Load With Micro-Finite Element Analysis Models Based on Three-dimensional Peripheral Quantitative Computed Tomography Images. Bone 30(6), 842–848 (2002)